J|A|C|S
ARTICLES

Published on Web 07/30/2010

Hydrogen Bonds between Nitrogen Donors and the Semiquinone in the Q_B Site of Bacterial Reaction Centers

Erik Martin,[†] Rimma I. Samoilova,[‡] Kupala V. Narasimhulu,[§] Colin A. Wraight,*[,†] and Sergei A. Dikanov*[,§]

Center for Biophysics & Computational Biology, University of Illinois at Urbana−Champaign, Urbana, Illinois 61801, Institute of Chemical Kinetics and Combustion, Russian Academy of Sciences, Novosibirsk 630090, Russia, and Department of Veterinary Clinical Medicine, University of Illinois at Urbana−Champaign, Urbana, Illinois 61801

Received May 13, 2010; E-mail: cwraight@illinois.edu; dikanov@illinois.edu

Abstract: Photosynthetic reaction centers from *Rhodobacter sphaeroides* have identical ubiquinone-10 molecules functioning as primary (Q_A) and secondary (Q_B) electron acceptors. X-band 2D pulsed EPR spectroscopy, called HYSCORE, was applied to study the interaction of the Q_B site semiquinone with nitrogens from the local protein environment in natural and ^{15}N uniformly labeled reactions centers. ^{14}N and ^{15}N HYSCORE spectra of the Q_B semiquinone show the interaction with two nitrogens carrying transferred unpaired spin density. Quadrupole coupling constants estimated from ^{14}N HYSCORE spectra indicate them to be a protonated nitrogen of an imidazole residue and amide nitrogen of a peptide group. ^{15}N HYSCORE spectra allowed estimation of the isotropic and anisotropic couplings with these nitrogens. From these data, we calculated the unpaired spin density transferred onto 2s and 2p orbitals of nitrogen and analyzed the contribution of different factors to the anisotropic hyperfine tensors. The hyperfine coupling of other protein nitrogens with the semiquinone is weak (<0.1 MHz). These results clearly indicate that the Q_B semiquinone forms hydrogen bonds with *two* nitrogens and provide quantitative characteristics of the hyperfine couplings with these nitrogens, which can be used in theoretical modeling of the Q_B site. On the basis of the quadrupole coupling constant, one nitrogen can only be assigned to N_δ of His-L190, consistent with all existing structures. However, we cannot specify between two candidates the residue corresponding to the second nitrogen. Further work employing multifrequency spectroscopic approaches or selective isotope labeling would be desirable for unambiguous assignment of this nitrogen.

Introduction

In the purple photosynthetic bacterium, *Rhodobacter (Rba.) sphaeroides*, the reaction center (RC) functions to couple the absorption of light to the generation of electrochemical free energy. Light activation results in sequential electron transfer through a series of cofactors of graded low potential. *Rba. sphaeroides* presents a unique opportunity to study the effect of protein structure on cofactor redox potential. The final two cofactors in this species of RC are chemically identical ubiquinone-10 molecules with dramatically different function.[1−7]

The primary acceptor Q_A is a tightly bound prosthetic group, while the secondary quinone Q_B serves as a mobile carrier of two reducing equivalents. The photochemistry of the RC involves light-induced charge separation at a dimer of bacteriochlorophyll followed by electron transfer through bacteriopheophytin to generate Q_A^-. The two-electron chemistry of the secondary quinone requires sequential electron transfer from Q_A^- to the Q_B site, through a protein medium dominated by an $Fe^{II}-(His)_4$ complex.[1,2,4,6,7] The two charge-neutral forms—oxidized Q_B and doubly reduced, protonated Q_BH_2—are able to diffuse in and out of the binding pocket. However, the semiquinone (SQ) intermediate, Q_B^-, is stabilized and is tightly bound. It is reasonable to expect that hydrogen bonding to the SQ contributes to the stability of this species.

Since the first reaction center crystal structure in 1985, a plethora of subsequent structures have suggested potential hydrogen bonding features. Despite this fact, significant uncertainties in the conformations of the two quinones and in the significance of the variable location of Q_B in the protein still exist. Consequently, the influence of structure on quinone function is only crudely understood.[7]

Crystal structures show that Q_B can occupy at least two different configurations, a tightly bound proximal position and

[†] Center for Biophysics & Computational Biology, University of Illinois at Urbana−Champaign.
[‡] Russian Academy of Sciences.
[§] Department of Veterinary Clinical Medicine, University of Illinois at Urbana−Champaign.

(1) Okamura, M. Y.; Paddock, M. L.; Graige, M. S.; Feher, G. *Biochim. Biophys. Acta* **2000**, *1458*, 148–163.
(2) Wraight, C. A. *Front. Biosci.* **2004**, *9*, 309–337.
(3) Lancaster, C. R. D. *FEBS Lett.* **1998**, *545*, 52–60.
(4) Lancaster, C. R. D.; Ermler, U.; Michel, H. In *Anoxygenic Photosynthetic Bacteria*; Blankenship, R. E., Madigan, M. T., Bauer, C. E., Eds.; Kluwer Academic Publishers: Dordrecht, The Netherlands, 1995; pp 503−526.
(5) Xu, Q.; Gunner, M. R. *Biochemistry* **2002**, *41*, 2694–2701.
(6) Stowell, M. H.; McPhillips, T. M.; Rees, D. C.; Soltis, S. M.; Abresch, E.; Feher, G. *Science* **1997**, *276*, 812–816.
(7) Wraight, C. A.; Gunner, M. R. In *The Purple Phototrophic Bacteria*; Hunter, C. N., Daldal, F., Thurnauer, M. C., Beatty, J. T., Eds.; Springer: Berlin, 2009; pp 379−405.

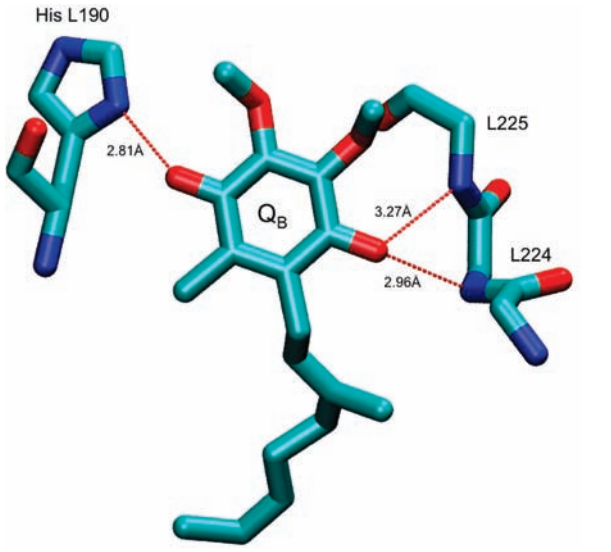

Figure 1. Residues involved in binding and stabilization of Q_B^- in *Rba. sphaeroides* reaction centers. Coordinates from pdb 1aig.[6] There are no crystallographically defined waters in the immediate Q_B pocket when the occupant is proximal to the Fe−histidine complex.

a distal position more distant from the $Fe^{II}-(His)_4$ complex.[6,8] Q_B is always seen to occupy the proximal location in preparations where the RC was frozen under illumination, indicating that it is this conformation which traps the semiquinone Q_B^- state. Structures with Q_B in the proximal position (Figure 1) show N_δ of His-190 (an Fe ligand) as a H-bond donor to the C_4 carbonyl and backbone −NH groups from Ile-L224 and/or Gly-L225 as potential H-bond donors to the C_1 carbonyl.[6] Additionally, the hydroxyl from Ser-L223 is thought to form a hydrogen bond with either the quinone carbonyl, especially in the semiquinone state, or Asp-L213.[5,7,9] In addition to the hydrogen bonds between the two carbonyls of Q_B and N_δ of His-L190 and backbone −NH, a weaker hydrogen bond from N−H of Thr-L226 to one methoxy group was inferred from analysis of a recent structure.[8] The distal position of Q_B is restrained by only a single hydrogen bond between one oxo group of Q_B and the nitrogen of Ile-L224.[6,8]

A complete picture of Q_B chemical reactivity and kinetic pathways cannot be answered by crystallography alone and requires a more complete knowledge of the SQ species at each site. The structural basis for modulation of the properties of the bound SQ by the protein can be revealed through the application of modern pulsed EPR methods.[7,10] Among quinone binding sites, the Q_A and Q_B sites have been some of the most thoroughly explored by ENDOR and 1D ESEEM.[9−15] However, the available data for hydrogen-bonded protons and nitrogen donors are still not complete due to limitations of 1D techniques. For instance, the hyperfine tensors for the exchangeable proton(s) involved in hydrogen bonds with carbonyls in the Q_B site are not determined, and the number of hydrogen-bonded nitrogens and their hyperfine couplings are uncertain. To resolve the existing uncertainties and to identify directly the nitrogens hydrogen bonded with the SQ in the Q_B site of the bacterial RC, we employed X-band 2D ESEEM (HYSCORE) in conjunction with uniform ^{15}N protein labeling.

Experimental Section

Sample Preparations. Bacteria were grown in Sistrom's medium with malate. Uniformly ^{15}N-labeled samples were created by substituting labeled ammonium sulfate obtained from Cambridge Isotopes in the Sistrom's medium. Reaction centers for this study were isolated from a His-tagged 2.4.1 strain by published procedures.[16] In order to remove the broad signal arising from semiquinone coupling to the high spin Fe^{2+}, Fe was biochemically replaced with diamagnetic Zn^{2+} according to the procedures outlined by Utschig et al.[17] After metal exchange, RCs were concentrated to ∼300−400 μM.

Concentrated reaction centers were buffer exchanged by dilution in 10 mL of 10 mM Tris, pH 7.9, 20 μM EDTA, and 0.03% Triton-X-100 detergent. For deuterium-exchanged samples, the dilutions were incubated at 4 °C for 24 h to ensure complete exchange. Following dilution, samples were reconcentrated to volumes equivalent to the starting volume. RC preparations were assayed for Q_B function, with added ubiquinone-10, by measuring the kinetics of charge recombination following a flash.[1,2,5] The slow phase ($t_{1/2} \approx 1$ s), indicative of Q_B activity, was routinely greater than 80%.

To prepare samples for EPR, buffer-exchanged RCs were combined with ∼3 equiv of horse heart ferrocytochrome *c*, ∼3 equiv of ubiquinone-10, and 10% glycerol in the EPR tubes. The Q_B semiquinone was created by a single laser flash at 532 nm, after which the samples were promptly frozen in liquid nitrogen.[10] The cytochrome *c* rapidly reduces the photo-oxidized primary donor of the RC and traps the transferred electron on the quinone. The X- and Q-band EPR spectra of the Q_B semiquinone possess characteristics consistent with those previously reported.[10]

EPR and ESEEM Experiments. The CW EPR measurements were performed on an X-band Varian EPR-E122 spectrometer and a Q-band Bruker ELEXSYS 580 equipped with a separate Q-band microwave bridge and cavity operating at 100 kHz modulation frequency. Pulsed EPR measurements were carried out using an X-band Bruker ELEXSYS E580 spectrometer with an Oxford CF 935 cryostat at 70 K. Several types of ESEEM experiments with different pulse sequences were employed, with appropriate phase-cycling schemes to eliminate unwanted features from experimental echo envelopes. Among them are one- (1D) and two-dimensional (2D) three- and four-pulse sequences. In the 1D three-pulse experiment ($\pi/2$-τ-$\pi/2$-T-$\pi/2$-τ-echo), the intensity of the stimulated echo signal after the third pulse is recorded as a function of time, T, at constant time, τ. The set of three-pulse envelopes recorded at different τ values forms a 2D three-pulse data set (as in Figure 2 of this article). In the 2D four-pulse experiment ($\pi/2$-τ-$\pi/2$-t_1-π-t_2-$\pi/2$-τ-echo, also called HYSCORE[18]), the intensity of the echo after the fourth pulse was measured with t_2 and t_1 varied and τ constant. The length of a $\pi/2$ pulse was nominally 16 ns and a π pulse 32 ns. The repetition rate of pulse sequences was 1000 Hz. HYSCORE data were collected in the form of 2D time-domain patterns containing 256 × 256 points with steps of 20 or 32 ns.

(8) Koepke, J.; Krammer, E. M.; Klingen, A. R.; Sebban, P.; Ullmann, G. M.; Fritzsch, G. *J. Mol. Biol.* **2007**, *371*, 396–409.
(9) Paddock, M. L.; Flores, M.; Isaacson, R.; Chang, C.; Abresch, E. C.; Okamura, M. Y. *Biochemistry* **2007**, *46*, 8234–8243.
(10) Lubitz, W.; Feher, G. *Appl. Magn. Reson.* **1999**, *17*, 1–48.
(11) Flores, M.; Isaacson, R.; Abresch, E.; Calvo, R.; Lubitz, W.; Feher, G. *Biophys. J.* **2007**, *92*, 671–682.
(12) Flores, M.; Isaacson, R.; Abresch, E.; Calvo, R.; Lubitz, W.; Feher, G. *Biophys. J.* **2006**, *90*, 3356–3362.
(13) Bosch, M. K.; Gast, P.; Hoff, A. J.; Spoyalov, A. P.; Tsvetkov, Yu. D. *Chem. Phys. Lett.* **1995**, *239*, 306–312.
(14) Spoyalov, A. P.; Hulsebosch, R. J.; Shochat, S.; Gast, P.; Hoff, A. J. *Chem. Phys. Lett.* **1996**, *263*, 715–720.
(15) Lendzian, F.; Rautter, J.; Käss, H.; Gardiner, A.; Lubitz, W. *Ber. Bunsen-Ges. Phys. Chem.* **1996**, *100*, 2036–2040.
(16) Goldsmith, J. O.; Boxer, S. G. *Biochim. Biophys. Acta* **1996**, *1276*, 171–175.
(17) Utschig, L. M.; Greenfield, S. R.; Tang, J.; Laible, P. D.; Thurnauer, M. C. *Biochemistry* **1997**, *36*, 8548–8558.
(18) Höfer, P.; Grupp, A.; Nebenführ, H.; Mehring, M. M. *Chem. Phys. Lett.* **1986**, *132*, 279–284.

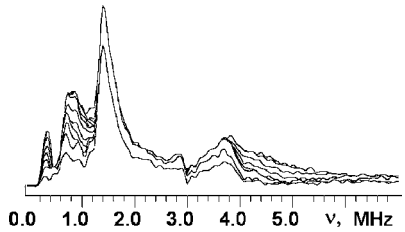

Figure 2. Stacked plots of three-pulse ESEEM spectra of the SQ at the Q_B site of *Rba. sphaeroides* reaction centers. The spectra show modulus Fourier transforms along the time T (between second and third microwave pulses) axis at different times τ. The initial time τ (between first and second pulses) is 100 ns in the farthest trace and was increased by 16 ns in successive traces. The microwave frequency was 9.705 GHz, and the magnetic field was 346.1 mT.

Spectral processing of ESEEM patterns, including subtraction of the relaxation decay (fitting by polynomials of 3−4 degree), apodization (Hamming window), zero filling, and fast Fourier transformation (FT), was performed using Bruker WIN-EPR software.

Spectral Simulations. HYSCORE simulations were performed using home-written software based on the density matrix formalism in the approximation of ideal strong pulses and taking into account the phase interference effects in powder HYSCORE spectra. The software uses numerical diagonalization of the full spin Hamiltonian for an electron spin $S = 1/2$ interacting with one nuclear spin up to $I = 9/2$ and taking into account their hyperfine and nuclear quadrupole interactions with arbitrary orientations of the tensors in the electron g-tensor frame. Orientation averaging for powder spectra is done taking into account orientation selectivity in HYSCORE experiment, for example, using the excitation bandwidth of microwave pulses and the g-factor anisotropy. This software was developed by Dr. Alexei Tyryshkin (now at Princeton University) and can be used on a PC without any additional commercial software.

The "Cancellation Condition" in ^{14}N ESEEM Spectra. Because of the $I = 1$ spin, and the quadrupole interactions resulting from this, the ^{14}N nucleus can produce up to six lines in an ESEEM spectrum, three from each of the two electron spin manifolds with $m_S = +1/2$ or $-1/2$. In measurements of amorphous (powder) samples, such as the frozen suspensions of RCs used in this work, not all transitions contribute equally to the spectrum due to different orientation dependences. The type of spectrum expected from ^{14}N with predominantly isotropic hyperfine coupling, ^{14}A, is governed by the ratio between the effective nuclear frequency in each manifold, given by $\nu_{ef\pm} = |^{14}\nu_N \pm |^{14}A|/2|$ ($^{14}\nu_N$ is the Zeeman frequency of ^{14}N), and the quadrupole coupling constant, given by $K = e^2qQ/4h$.[19,20]

If $\nu_{ef\pm} \cong 0$ (called a "cancellation condition" because $^{14}\nu_N \cong |^{14}A|/2$), then the three nuclear frequencies from the corresponding manifold will be close to the three pure (or zero-field) nuclear quadrupole resonance (nqr) frequencies of ^{14}N. In this case, three narrow peaks at the frequencies ν_+, ν_-, and ν_o will appear in the powder ESEEM spectra, with the property $\nu_+ = \nu_- + \nu_o$:

$$\nu_+ = K(3 + \eta);\ \nu_- = K(3 - \eta);\ \nu_0 = 2K\eta \qquad (1)$$

The frequencies, described by eq 1 can appear in spectra up to a ratio of $\nu_{ef\pm}/K \sim 0.75-1$ but are broadened as this value departs from 0.[19,20] The term η is an asymmetry parameter.

If $\nu_{ef\pm}/K > 1$, only a single line is expected from each corresponding manifold without any pronounced orientation dependence. This line is produced by a transition at the maximum frequency, which is actually a double-quantum (dq) transition between the two outer states with $m_I = -1$ and $+1$. The frequency of this transition is well described by eq 2:

$$\nu_{dq\pm} = 2[\nu_{ef\pm}^2 + \kappa]^{1/2} \qquad (2)$$

where $\kappa = K^2(3 + \eta^2)$. Two other single-quantum (sq) transitions, involving the central level with $m_I = 0$, have a significant orientation dependence from quadrupole interaction and can produce broad lines of low intensity at varying frequencies in the powder spectra.

A three-pulse ESEEM spectrum near the cancellation condition is expected to consist of four lines: three narrow lines at zero-field nqr frequencies from the manifold with $\nu_{ef} \sim 0$, described by eq 1, and one double-quantum transition from the opposite manifold, described by eq 2. The corresponding HYSCORE spectrum will exhibit cross-peaks correlating ν_o, ν_-, and ν_+ with ν_{dq}, thus indicating that they belong to different manifolds. The cross-peaks' contour line shape should be a narrow straight-line segment parallel to one coordinate axis and normal to the other.

At large deviations from cancellation conditions, two resolved lines from double-quantum transitions belonging to opposite m_S manifolds should present in a three-pulse spectrum. These two transitions will produce two cross-peaks, correlating ν_{dq+} and ν_{dq-}, in the HYSCORE spectrum. The cross-peaks can possess arbitrary contour orientation and shape depending on the particular values of the hyperfine and quadrupole tensors and their relative orientation. Other cross-peaks, correlating sq−sq and dq−sq transitions, are usually absent in the spectrum or possess low intensity and significantly poorer resolution.

Results

The X-band three-pulse ^{14}N ESEEM spectrum of the Q_B SQ in wild-type RC is shown in Figure 2 and is quite distinct from the ^{14}N ESEEM spectrum of the Q_A SQ.[13] The Q_B SQ spectrum is dominated by a line at 1.5 MHz. At lower frequency, there is a peak at ∼0.3 MHz and a feature around 0.7 MHz that appears to contain overlapping peaks. At higher frequencies, there are a weak peak at 2.9 MHz and a broad feature around 3.8 MHz. The shape of this spectrum suggests the SQ is coupled to more than one ^{14}N nucleus.

Additional evidence for this assertion can be obtained from 2D ESEEM (HYSCORE) spectra. The corresponding HYSCORE spectrum of the Q_B SQ (Figure 3) exhibits intense and extended cross-ridges **1** possessing a maximum at (3.96, 1.51) MHz, indicating that these two frequencies are from opposite electron spin manifolds of the same nitrogen N1. There is a second pair of cross-peaks **2** with smaller intensity and approximately circular shape of small radius and correlating frequencies 3.86 and 2.98 MHz. We assign this pair of cross-peaks to another nitrogen N2.

The two pairs of cross-peaks **1** and **2** in the ^{14}N HYSCORE spectra probably correlate to double-quantum transitions from the $m_S = \pm 1/2$ manifolds of two nuclei N1 and N2. Using these frequencies and eq 2, the hyperfine coupling A and quadrupole parameter $\kappa = K^2(3 + \eta^2)$ are estimated to be $^{14}A_1 = 1.57$ MHz and $\kappa = 0.49$ MHz^2, and $^{14}A_2 = 0.7$ MHz and $\kappa = 1.7$ MHz^2 for cross-peaks **1** and **2**, respectively (with Zeeman frequency $^{14}\nu_N = 1.065$ MHz). The values for κ lead to the quadrupolar coupling constant $K = e^2qQ/4h \sim 0.35-0.40$ MHz for N1 and ∼0.65−0.75 MHz for N2 when η varies between 0 and 1 ($0 \leq \eta \leq 1$). The smaller K value of ∼0.35−0.40 MHz is consistent with a protonated imidazole nitrogen.[21] The K value of ∼0.65−0.75 MHz is in line with a peptide nitrogen carrying

(19) Dikanov, S. A.; Tsvetkov, Yu.D.; Bowman, M. K.; Astashkin, A. V. *Chem. Phys. Lett.* **1982**, *90*, 149–153.
(20) Flanagan, H.; Singel, D. J. *J. Chem. Phys.* **1987**, *87*, 5606–5616.
(21) Dikanov, S. A.; Holland, J. T.; Endeward, B.; Kolling, D. R. J.; Samoilova, R. I.; Prisner, Th. F.; Crofts, A. R. *J. Biol. Chem.* **2007**, *282*, 25831–25841 (see Table 2).

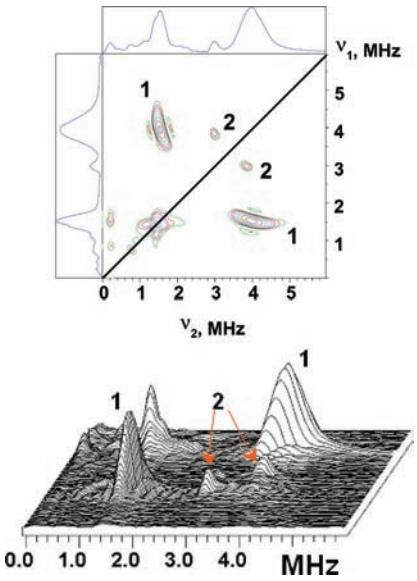

Figure 3. Contour (top) and stacked (bottom) presentations of the ^{14}N HYSCORE spectrum of the SQ at the Q_B site of the *Rba. sphaeroides* reaction center (magnetic field 346.1 mT, time between first and second pulses $\tau = 136$ ns, microwave frequency 9.705 GHz).

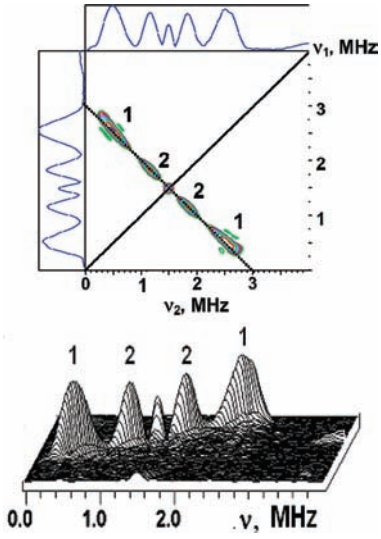

Figure 4. Contour (top) and stacked (bottom) presentations of the HYSCORE spectrum of the SQ at the Q_B site of uniformly ^{15}N-labeled reaction centers (magnetic field 345.4 mT, time between first and second pulses $\tau = 136$ ns, microwave frequency 9.688 GHz).

unpaired spin density transferred via a N−H−O-type hydrogen bond(s).[22] These parameter values clearly do not conform closely to the cancellation condition.

The assignment of the cross-peaks in the ^{14}N spectrum to two nitrogens is further supported by experiments with uniformly ^{15}N-labeled RCs. The ^{15}N HYSCORE spectrum (Figure 4) exhibits a narrow diagonal peak at ($^{15}\nu_N$,$^{15}\nu_N$) from weakly coupled nitrogens and two pairs of cross-peaks **1** and **2**. They are located symmetrically around the diagonal peak, along the antidiagonal, with maxima at (2.53, 0.49) MHz (**1**) and (1.83, 1.16) MHz (**2**), which correspond to hyperfine couplings $^{15}A_1 = 2.04$ MHz and $^{15}A_2 = 0.67$ MHz. The hyperfine couplings recalculated for ^{14}N are equal to 1.43 and 0.49 MHz, respectively, in reasonable agreement with the couplings determined from ^{14}N HYSCORE. The difference between the couplings derived from the two HYSCORE spectra results from different factors influencing the position of the line maximum in powder spectra for a ^{14}N and ^{15}N nucleus.

Discussion

Relation to Published Results. Lendzian et al. have previously reported the three-pulse ESEEM spectrum of the Q_B site SQ in *Rba. sphaeroides*.[15] Their spectrum, recorded with time $\tau =$ 120 ns, is consistent with the spectrum shown in Figure 2 in terms of the presence of the intense ~1.5 MHz peak and dq transition at ~4 MHz. These features were assigned to a single nitrogen, N_δ of the histidine (L190), and were interpreted assuming fulfillment of the exact cancellation condition for its ^{14}N nucleus. Cancellation allows for the appearance of three narrow intense peaks at frequencies corresponding to the ^{14}N pure nqr triplet (eq 1). The interpretation given in ref 15 suggests that the intense ~1.5 MHz line belongs to the ν_+ transition. However, the features assigned to the two additional quadrupole frequencies ν_- and ν_o are comparable with the noise level in other parts of the spectrum, and their frequencies are not reported. Instead, the article provides characteristics of the nqi tensor, quadrupole coupling constant $e^2qQ/h = 1.65$ MHz ($K = 0.4125$ MHz) and asymmetry parameter $\eta = 0.61$, which allow one to calculate nqr frequencies as 1.49, 0.99, and 0.50 MHz. Our spectra recorded at different times τ do not show the appearance of peaks at these frequencies. In addition, the shapes of the cross-peaks **1** in the HYSCORE spectrum have a curved contour shape in contrast to the straight segment parallel to the coordinate axis expected for the cancellation condition, when nqr frequencies do not show any orientational dependence. Thus, these observations indicate that the cancellation condition is not fulfilled for nitrogen N1 in the X-band.

This conclusion also follows from the value of the hyperfine coupling $^{14}A_1 \sim 1.5$ MHz, estimated from ^{14}N and ^{15}N HYSCORE spectra, which significantly deviates from $2^{14}\nu_N \sim 2.13$ MHz in magnetic field 346.1 mT. Taking a typical value of $K \sim 0.38-40$ MHz, one can find that $|^{14}\nu_N - {}^{14}A/2|/K \cong 0.83$, which corresponds to significant deviation from cancellation. This would yield a spectrum with two dominating dq transitions from opposite m_S manifolds, as seen at 1.5 and 3.8 MHz in three-pulse and HYSCORE spectra. The deviation from cancellation is even larger for N2 with smaller hyperfine coupling $^{14}A_2 \sim 0.6$ MHz and $|^{14}\nu_N - {}^{14}A/2|/K \cong 1.1$. This analysis suggests that the cancellation condition for nitrogens N1 and N2, required for complete determination of nuclear quadrupole tensor, could be achieved at lower microwave frequencies, yielding smaller $^{14}\nu_N$.

Simulations of ^{15}N HYSCORE Spectra. In order to characterize the hyperfine tensor for N1 and N2 more precisely, we have performed simulations of the ^{15}N HYSCORE spectra of the Q_B SQ. The major methodological problem of the powder HYSCORE analysis, in this case, is that the cross-peaks N1 and N2 possess highly symmetrical line shapes with the maximum corresponding to the undefined orientation of the magnetic field relative to the principal axes of the hyperfine tensor and total "visible" width about ~0.70 MHz (N1) and ~0.55 MHz (N2) along the antidiagonal. The intensity is suppressed at the cross-peak wings corresponding to field orientations along or near the axes with maximum and minimum principal values of the tensor. The relative signs of the isotropic and anisotropic

(22) Yap, L. L.; Samoilova, R. I.; Gennis, R. B.; Dikanov, S. A. *J. Biol. Chem.* **2006**, *281*, 16879–16887, and references therein.

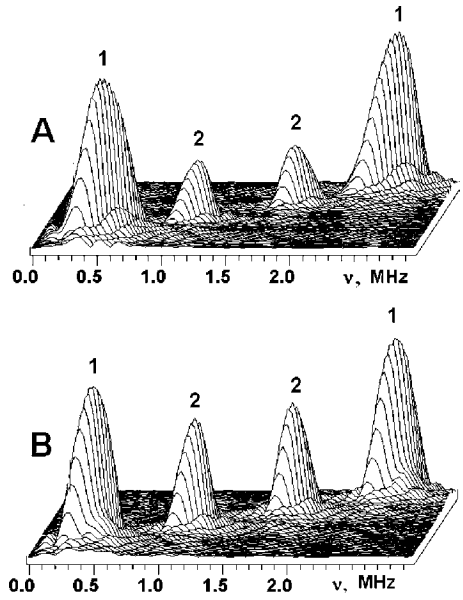

Figure 5. ^{15}N HYSCORE spectra in stacked presentation: (A) simulated with axial hyperfine tensors ($a - T$, $a - T$, $a + 2T$) for both nuclei with $a = 2.1$ MHz, $T = -0.35$ MHz (N1) and $a = 0.65$ MHz, $T = 0.2$ MHz (N2). (B) Simulated with rhombic hyperfine tensors ($a - T_1$, $a - T_2$, $a + T_3$): $a = 2.1$ MHz, $T_3 = T_1 = 0.4$ MHz, $T_2 = 0$ MHz (N1) and $a = 0.65$ MHz, $T_1 = 0.25$ MHz, $T_2/T_1 = 0.5$ (N2). Hyperfine parameters are for ^{15}N isotope.

components and symmetry of the tensor (i.e., axial or rhombic) are also uncertain from the line shape.

Initial estimate of the isotropic (a) and anisotropic (T) components of the hyperfine tensor was made assuming typical axial symmetry, with principal components ($a - T$, $a - T$, $a + 2T$), and linear fitting of the cross-peaks in the coordinates $(\nu_1)^2$ versus $(\nu_2)^2$.[23] Adjustment of the estimated axial parameters was performed through numerical simulations of the spectra. The location of the line maximum and width of the cross-peaks along the antidiagonal were used as criteria for the comparison of simulated and experimental spectra for each nucleus. In simulations assuming axial symmetry, the intensities of the peaks N1 are several times larger than peaks N2 in the 3D presentation of the spectrum obtained by summing two individually calculated spectra (Figure 5A). The intensities of the N1 peaks decrease significantly with increasing rhombicity of the hyperfine anisotropy. The spectra simulated for the fully rhombic anisotropic tensor ($-T$, 0, T) with the same isotropic constant and the same order of T show an intensity ratio more consistent with experimental results (Figure 5B).

Additionally, it is important to note that the spectra shown in Figure 5 are obtained as a sum of individually calculated spectra and demonstrate the influence of the aforementioned factors on line shape and intensity of the cross-peaks. However, ideal HYSCORE simulations would consider the interaction of electron spin simultaneously with two nuclei whose hyperfine tensors are defined in the same coordinate system. In this treatment, the simulations would depend on the orientation of the principal axes of two individual hyperfine tensors in the SQ g-tensor coordinate system or on the relative orientation of the principal axes of the hyperfine tensor in the approximation of an isotropic g-tensor. This approach, however, would significantly complicate the simulation procedure of the powder spectrum with addition of up to six angular parameters without significant improvement in the hyperfine couplings obtained. In addition, strong mutual influence of the two nuclei interacting with the unpaired electron on the shape and intensity of cross-peaks would suggest the appearance of multiple cross-peaks mixing frequencies of N1 and N2. Our spectra, however, do not show any such peaks indicating weak influence of cross-correlation.[24]

In summary, the spectral simulations provide isotropic constants 1.5 MHz (N1) and 0.45 MHz (N2) (± 0.02 MHz) consistent with the estimates obtained from experimental spectra. On the other hand, the absence of direct information about principal values of the anisotropic tensor from the powder line shape of ^{15}N HYSCORE spectra precludes its exact determination for N1 and N2. We can only conclude that tensors are probably rhombic ($-T_1$, $-T_2$, T_3), and the absolute value of their maximum components T_3 could vary between $\sim 0.3-0.5$ MHz (N1) and $0.21-0.28$ MHz (N2) when the ratio of the two smallest components T_2/T_1 changes from 0 to 1. All hyperfine parameters are recalculated for ^{14}N isotope.

A possible influence of the static distribution of hyperfine parameters on the line shape of the cross-peaks can be largely discounted. Analysis of the line shapes in the "single-crystal-like" Q-band ENDOR spectra from the protons of hydrogen bonds in the Q_A site of RC in *Rba. sphaeroides*[11] shows that the influence of this factor on the value of hyperfine coupling would not exceed $\pm 5\%$. This is substantially smaller than the uncertainty in the determination of the hyperfine tensor components from ^{15}N spectra and would not influence the analysis of the hyperfine tensors for N1 and N2 considered in the following section.

Analysis of the Hyperfine Tensors of N1 and N2. The existence of nonzero isotropic constants for the interacting nitrogens N1 and N2 indicates directly that unpaired electron spin density is transferred from the SQ onto these atoms. This implies the existence of atomic bridges (e.g., H-bonds). Isotropic hyperfine interaction for ^{14}N nuclei arises from unpaired 2s spin density, while unpaired 2p spin density contributes to the anisotropic hyperfine interaction.

The hyperfine couplings obtained from ^{15}N HYSCORE simulations allow estimation of the unpaired spin s and p populations for N1 and N2 based on the unit spin ^{14}N atomic hyperfine constant $a = 1811$ MHz and $T_p = 55.5$ MHz[25] (or 111 MHz for the largest component of the anisotropic tensor, which can be used for significantly rhombic tensors), suggesting that the anisotropic hyperfine coupling is fully accounted for by the transferred unpaired 2p spin density. This analysis yields s and p populations of 0.83×10^{-3} and $(2.7-4.5) \times 10^{-3}$ (p/s $= 3.2-5.4$) for N1 and 0.25×10^{-3} and $(1.9-2.5) \times 10^{-3}$ (p/s $= 7.6-10$) for N2. These populations are obtained without regard to the hybridization of the nitrogen atomic orbitals.

The $2s^2 2p^3$ valence shell of the nitrogen atom consists of four orbitals, one of which is a lone-pair orbital. The His-L190 N_δ 2s orbital is involved with p in sp^2 hybridization.[26] The amide nitrogen of the planar peptide probably has the same hybridiza-

(23) Dikanov, S. A.; Bowman, M. K. *J. Magn. Reson., Ser. A* **1995**, *116*, 125–128.

(24) Stoll, S.; Calle, C.; Mitrikas, G.; Schweiger, A. *J. Magn. Reson.* **2005**, *177*, 93–101.

(25) Morton, J. R.; Preston, K. F. *J. Magn. Reson.* **1978**, *30*, 577–582.

(26) McDowell, C. A.; Naito, A.; Sastry, D. L.; Takegoshi, K. *J. Magn. Reson.* **1986**, *69*, 283–292.

Table 1. Estimated T_{dd} and T_p Contributions to the Anisotropic Hyperfine Tensor

nitrogen	N···O distance (Å)	^{14}N T_{dd} (MHz)	^{14}N T_p (MHz)	$2(T_{dd} + T_p)$ (MHz)
His-L190 (Q_B)	2.81	0.048	0.046	0.19
Ile-L224 (Q_B)	2.96	0.037	0.014	0.10
Gly-L225 (Q_B)	3.27	0.027	0.014	0.08
His-M219 (Q_A)[a]	2.67	0.043	0.081	0.24
Ala-M260 (Q_A)[a]	2.81	0.051	0.042	0.19

[a] From refs 33 and 35.

tion. The wave function of the hybridized orbital forming the N−H bond can be expressed as[27]

$$\psi = c_s|2s> + c_p|2p_x>$$
$$c_s^2 + c_p^2 = 1 \quad (3)$$

For imidazole, the c_s^2 population of the s orbital is determined by $\cot^2\theta$, where 2θ is the CNC angle of ∼108−110°. This gives $c_s^2 \sim 1/2$, implying that a similar spin density c_p^2 resides on the 2p orbital. For ideal sp^2 hybridization geometry where $2\theta = 120°$, c_s^2 and c_p^2 population coefficients are 1/3 and 2/3, respectively. Thus, sp^2 hybridization typically leads to p/s ratios of 1−2. The p/s ratios estimated above from the experimental nitrogen hyperfine couplings of Q_B SQ correspond to substantially larger "effective" p populations than expected for a sp^2 hybrid orbital, suggesting additional factors contributing to the anisotropic hyperfine tensor.

In contrast to the isotropic component, the anisotropic hyperfine tensor of the nitrogen hydrogen bonded with SQ oxygen is the result of at least two factors: dipole−dipole coupling and spin transfer. The dipole−dipole contribution to the hyperfine tensor is determined chiefly by the O···N distance. The typical approach used for estimation of this contribution considers the dipole−dipole interaction between the nucleus and the unpaired spin density localized on the nearest carbonyl oxygen of the SQ:

$$T_{dd} = \rho_O(g_e g_I \beta_e \beta_I / hr^3) = \rho_O(b/r^3) \quad (4)$$

where ρ_O is the π spin density at the quinone oxygen and r is the O···N distance, g_e, g_I, β_e, β_I are the electron and nuclear g-factors and Bohr and nuclear magnetons, respectively, $b = 8$ (for ^{15}N) and 5.54 (for ^{14}N). The value ρ_O is estimated to be ∼0.187 (O_1) and 0.169 (O_4) from experiments with ^{17}O-labeled SQs in the Q_B site of the RC.[10]

Using eq 4, one can estimate T_{dd} values for ^{14}N nitrogens of His-L190, Leu-L224, and Gly-L225 potentially involved in H-bonds with the Q_B SQ (Figure 1). Those are shown in Table 1 and do not exceed the value ∼0.05 MHz even for the nitrogen with the shortest distance of 2.81 Å. Unpaired spin density transferred onto the 2p orbital determines the second contribution to the anisotropic tensor. For a spin density $\rho_p \sim 0.83 \times 10^{-3}$ and 0.25×10^{-3} on the 2p orbital, this contribution is $T_p \sim$ 0.046 and 0.014 MHz. However, individual $\boldsymbol{T}_{dd}$ and $\boldsymbol{T}_p$ tensors possess different principal axes, and in order to derive the total anisotropic tensor, $\boldsymbol{T}$, the contributing tensors $\boldsymbol{T}_{dd}$ and $\boldsymbol{T}_p$ need to be defined in the same coordinate system. This introduces the rhombicity into the total tensor, despite the fact that the interaction with each individual tensor is axial in the approximations considered. In addition, the total principal values would be smaller than a simple sum of the two contributions. Thus, the upper limit of the largest principal value $T_3 < 2(T_{dd} + T_p)$ estimated for the tensor $\boldsymbol{T} = \boldsymbol{T}_{dd} + \boldsymbol{T}_p$ (Table 1) should not exceed 0.2 MHz for N1 and 0.12 MHz for N2. Values determined from HYSCORE analysis (0.3−0.5 and 0.21−0.28 MHz) substantially exceed this theoretical ceiling. In order to mimic the experimental data in the model suggested, we would need to assume a 2−4-fold increase in the T_{dd} contribution to the total tensor for N1 and N2, leading to an unrealistic 1.26−1.59 fold shortening of the H-bond distance inferred from crystal structures. An alternative explanation of the discrepancy is considered below, in terms of the nitrogen hyperfine tensors observed in related systems, experimentally and from calculations.

The higher than expected p/s ratio from sp^2 orbital hybridization is fairly typical for nitrogen atoms hydrogen bonded with SQs and for remote nitrogens of imidazole coordinating paramagnetic copper(II) ions (Table 2). In both cases, dipole−dipole and spin density transfer mechanisms contribute to the anisotropic hyperfine tensor. The ^{14}N hyperfine tensors in Cu(II)-doped L-histidine hydrochloride and Cu(II)-doped zinc bis(1,2-dimethyl imidazole) dichloride were measured by single-crystal ESEEM and provide information about orientation of the principal axes. The data shown in Table 2 indicate that a simple model of unpaired spin density location on hybrid orbital (3) of nitrogen is not sufficient, and the presence of additional unpaired p spin density on other orbital(s) could be suggested. In particular, for the planar imidazole and peptide groups, the lone-pair orbital is pure π orbital without any s character. The analysis of the nuclear quadrupole tensor indicates that the electronic population of this orbital is less than 2, especially for the nitrogen involved in H-bond formation.[28] Therefore, the p unpaired spin density on this orbital would not influence the observed isotropic hyperfine coupling but could give substantial contribution to the anisotropic tensor.

The localization of unpaired spin density on a pure p orbital of nitrogen is consistent with two possible mechanisms of the spin density transfer from semiquinone on hydrogen-bonded molecules discussed previously.[30] Spin density can be transferred through spin polarization via the s orbital of the hydrogen atom onto the next atom, that is, nitrogen in this case, or by direct spin delocalization of the π-electron spin from the oxygen atom. Theoretical calculations of unpaired spin density transfer onto the nitrogens hydrogen bonded with a radical oxygen are very limited. Hybrid density functional calculations exist for an imidazole H-bonded to a phenol radical. These suggest that spin polarization through the H-bonded proton transfers spin density to the nitrogen nucleus from the oxygen π spin density.[34] However, the calculations show very small anisotropy of the hyperfine coupling, on the order of 0−0.1 MHz, despite isotropic coupling values up to 1 MHz.

(27) McDowell, C. A.; Naito, A.; Sastry, D. L.; Cui, Y. U.; Sha, K.; Yu, S. X. *J. Mol. Struct.* **1989**, *195*, 361–381.
(28) Colaneri, M. J.; Peisach, J. *J. Am. Chem. Soc.* **1992**, *114*, 5335–5341.
(29) Colaneri, M. J.; Potenza, J. A.; Schugar, H. J.; Peisach, J. *J. Am. Chem. Soc.* **1990**, *112*, 9451–9458.
(30) Deligiannakis, Y.; Hanley, J.; Rutherford, A. W. *J. Am. Chem. Soc.* **1999**, *121*, 7653–7664.
(31) Dikanov, S. A.; Holland, J. T.; Endeward, B.; Kolling, D. R. J.; Samoilova, R. I.; Prisner, Th. F.; Crofts, A. R. *J. Biol. Chem.* **2007**, *282*, 25831–25841.
(32) Grimaldi, S.; Arias-Cartin, R.; Lanciano, P.; Lyubenova, S.; Endeward, B.; Prisner, Th. F.; Magalon, A.; Guigliarelli, B. *J. Biol. Chem.* **2010**, *285*, 179–187.
(33) Fritscher, J.; Prisner, T. F.; MacMillan, F. *Appl. Magn. Reson.* **2006**, *30*, 251–268.
(34) O'Malley, P. O. *J. Am. Chem. Soc.* **1998**, *120*, 11732–11737.
(35) Sinnecker, S.; Flores, M.; Lubitz, W. *Phys. Chem. Chem. Phys.* **2006**, *8*, 5659–5670.

Table 2. ^{14}N Hyperfine Tensors and p/s Ratio

system	nitrogen	*a*, MHz	anisotropic tensor, MHz	p/s	ref
Cu(II)-doped L-histidine hydrochloride	remote N_dH	1.35	−0.28, −0.09, 0.37	4.47	28
Cu(II)-doped zinc bis(1,2-dimethyl imidazole) dichloride	remote N−CH_3	1.42[a]	−0.20, −0.14, 0.33[a]	3.79	29
		1.35[a]	−0.19, −0.13, 0.33[a]	3.98	
SQ in Q_A site PSII	imidazole N−H	1.77[b]	−0.27, −0.27, 0.53[b]	4.88	30
		1.37[c]	−0.27, −0.27, 0.53[c]	6.30	
		1.87[d]	−0.37, −0.37, 0.73[d]	6.36	
		1.67[e]	−0.27, −0.27, 0.53[e]	5.17	
SQ in Q_A site PSII	peptide N−H	2.10[f]	−0.10, −0.40, 0.50[f]	3.87	30
		2.10[g]	−0.80, −0.80, 1.60[g]	12.42	
		2.10[h]	−0.40, −0.40, 0.80[h]	6.20	
SQ in Q_i site bc_1 complex	imidazole N−H	0.74	±(−0.12, −0.12, 0.24)	5.28	31
SQ in Q_D site nitrate reductase A	imidazole N−H	0.80	(−0.11, −0.11, 0.22)	4.48	32
SQ in Q_A site RC[i]	imidazole N−H	2.66	−0.31, −0.26, 0.58	3.55	33
		2.44	−0.25, −0.21, 0.47	3.13	
SQ in Q_A-site RC[i]	peptide N−H	1.38	−0.29, −0.27, 0.56	6.61	33
		1.09	−0.27, −0.26, 0.53	7.92	

[a] Two conformations are reported. [b] CN-treated PSII, pH 5.5. [c] Same as footnote b but pH 8.2. [d] With pH 11-treated PSII, pH 5.0. [e] Same as footnote d but pH 8.2. [f] CN-treated PSII, pH 7.2, no pH dependence. [g] With pH 11 treated PSII, pH 5.0. [h] Same as footnote g, but pH 7.2. [i] Calculated tensors; different computation models; see ref 33 for details.

More recent DFT calculations of the Q_A site SQ in bacterial reaction centers report the hyperfine tensors (Table 2) for N_δ of His-M219 and N_p of Ala-M260 without any discussion of the values obtained or of the mechanism of spin density transfer.[33] One can note, however, that the calculated isotropic and anisotropic components give high p/s ratios of 3.13−3.55 for N_δ of His-M219 and 6.61−7.92 for N_p of Ala-M260. These calculations used coordinates from the structure of Stowell et al.[6] and values of 2.66 and 2.84 Å for $N_\delta\cdots O_4$ and $N_p\cdots O_1$ distances in an optimized structure (in contrast to 2.91 and 2.83 Å read from the crystal structure).[33] Smaller values of 2.69 and 2.77−2.81 Å for $N_\delta\cdots O_4$ and $N_p\cdots O_1$ distances were also used in other computational work.[35] The estimated T_{dd} (the unpaired spin π densities 0.205 on O_1 and 0.148 on O_4 were used in calculations)[10] and T_p for the nitrogens interacting with the Q_A site SQ (Table 1) are of the same order as the values obtained for the Q_B site, and $2(T_{dd} + T_p)$ is far from the reported values of $T_3 \sim 0.47-0.58$ MHz[33] (Tables 1 and 2). These considerations show that further calculations with detailed analysis of spin density populations on different orbitals are needed for a quantitative understanding of the mechanism of spin density transfer and its relation to the geometry and strength of the H-bond. This is important in light of the role of H-bonds and the distribution of unpaired spin density on rates of electron and proton transfer.

Other Nitrogens. Powder-type ^{14}N ESEEM spectra, obtained with frozen protein solutions, do not usually show all of the ^{14}N nuclei that are magnetically coupled with the SQ. This is due to the influence of the nuclear quadrupole interaction.[31] To observe all of the nitrogens that are magnetically interacting with the unpaired electron spin of the SQ, it is necessary to use ^{15}N-labeled protein. The ^{15}N nucleus is a spin 1/2 system and does not possess the nuclear quadrupole moment that affects the ^{14}N ESEEM spectra. ^{15}N HYSCORE spectra, in addition to the peaks from N1 and N2 also seen in ^{14}N spectra, show a sharp diagonal peak with a width of ∼0.1 MHz. This peak can be assigned to multiple weak dipole−dipole interactions with other nitrogens in the protein environment. The failure to detect additional isotropic hyperfine couplings from N atoms other than N1 and N2 might suggest that no other N atom H-bonds with a SQ carbonyl oxygen. However, one cannot exclude the possibility of a hydrogen bond from N−H of Thr-L226 with the methoxy oxygen, proposed in ref 8, on the basis of the ^{15}N ESEEM. DFT calculations of spin density distribution in the anion radical of hydrogen-bonded ubiquinone in solution give a value of $\rho_\pi \sim 0.01-0.02$ for the methoxy oxygen, depending on the orientation of the methoxy group, which would give an estimate of the anisotropic hyperfine component $T < 0.005$ MHz. The width of the central peak allows the isotropic coupling of ∼0.1 MHz with ^{15}N nitrogen of this residue, which would need the transfer of spin density of $\sim 4 \times 10^{-5}$ onto this nucleus. This issue could be resolved using the selective ^{15}N labeling of the corresponding residue. Splittings of ∼0.1−0.15 MHz caused by unpaired spin density transferred to the protein nitrogens were previously resolved in ^{15}N HYSCORE for the semiquinone in the Q_H site of cytochrome bo_3 oxidase.[36]

Conclusion

^{14}N and ^{15}N HYSCORE data obtained in this work show that the Q_B semiquinone interacts with two nitrogens carrying transferred unpaired spin density. Quadrupole coupling constants $K \sim 0.35-0.40$ MHz (N1) and $K \sim 0.65-0.75$ MHz (N2) estimated from ^{14}N HYSCORE spectra indicate them to be protonated nitrogen of an imidazole residue and amide nitrogen of a peptide group, respectively. On the basis of the quadrupole coupling constant, N1 could only be assigned to N_δ of His-L190, consistent with all existing structures.[6,8] We cannot currently specify the residue corresponding to the N2 from two possible candidates from Ile-L224 and Gly-L225 suggested from X-ray structures.[6,8] Selective isotope labeling would be desirable for unambiguous experimental assignment of this nitrogen. However, according to private communication by Dr. P. O'Malley (University of Manchester, U.K.), computational QM/MM data indicate that the Q_B SQ forms a hydrogen bond with the peptide nitrogen of Gly-L225, in addition to a hydrogen bond with the nitrogen of His-L190, and provide the isotropic hyperfine couplings 0.5 and 1.2 MHz for these nitrogens, respectively, in very good agreement with the couplings determined in this work.

Thus, data obtained in the present work will be used for further modeling of the quinone environment in the SQ state in comparison with X-ray structures and will provide deeper experimental support for theoretical descriptions of the protein−semiquinone interaction in the Q_B site of the reaction center.

Acknowledgment. This investigation was supported by the NIH GM062954 Grant and DE-FG02-08ER15960 Grant from Chemical Sciences, Geosciences and Biosciences Division, Office of Basic Energy Sciences, Office of Sciences, U.S. DOE (S.A.D.), NSF Grant MCB0818121 (C.A.W.), and NCRR/NIH Grant S10-RR15878 for pulsed EPR instrumentation.

JA104134E

(36) Lin, M. T.; Samoilova, R. I.; Gennis, R. B.; Dikanov, S. A. *J. Am. Chem. Soc.* **2008**, *130*, 15768–15769.